Volume 4
Number 11
November 2024
Pages 1197–1324

Environmental Science
Atmospheres

rsc.li/esatmospheres

ISSN 2634-3606

ROYAL SOCIETY OF CHEMISTRY

PAPER
Sabine Lüchtrath *et al.*
Impact of atmospheric water-soluble iron on α-pinene-derived SOA formation and transformation in the presence of aqueous droplets

Environmental Science: Atmospheres

ROYAL SOCIETY OF CHEMISTRY

PAPER

View Article Online
View Journal | View Issue

Cite this: *Environ. Sci.: Atmos.*, 2024, **4**, 1218

Impact of atmospheric water-soluble iron on α-pinene-derived SOA formation and transformation in the presence of aqueous droplets†

Sabine Lüchtrath, *[a] Sven Klemer,[a] Clément Dubois, ‡[b] Christian George [b] and Andreas Held[a]

The impact of water-soluble atmospheric iron on formation, growth and aging of secondary organic aerosol (SOA) is a controversial subject in the literature. Iron chemistry drives Fenton reactions in the aqueous phase which is dependent on pH. Flow reactor experiments in the dark and under humid conditions were conducted to investigate systematically the influence of ferrous iron in the aqueous phase on α-pinene SOA by online physical analysis and offline high-resolution mass spectrometry. During the experiments increased SOA formation under conditions favorable for dark Fenton chemistry in the aqueous phase was observed. Furthermore, samples with an acidified and iron-containing aqueous phase showed a degradation of pinyl-diaterpenyl ($C_{17}H_{26}O_8$) ester which ages through oxidation *via* OH radicals and can thus be evidence for ongoing degradation processes of high molecular weight molecules by iron chemistry. Moreover, higher abundance of dimer MW338 ($C_{19}H_{30}O_5$) in the acidic sample affected by Fenton's chemistry was detected which is suggested to be formed *via* acid catalysis indicating competing acidity-driven reactions influencing SOA formation. Therefore, this study provides insight into the impact of aqueous phase iron on SOA formation and transformation under simulated natural conditions.

Received 2nd July 2024
Accepted 12th September 2024

DOI: 10.1039/d4ea00095a

rsc.li/esatmospheres

Environmental significance

Secondary organic aerosols (SOA) have a strong impact on the Earth's radiation budget and yet many SOA formation pathways in the atmospheric multiphase system have not been fully explored. In particular, iron as the most abundant transition metal of the Earth crust is capable of transforming organic compounds in the aqueous phase in photo- and redox reactions. However, the role of iron in atmospheric SOA formation and transformation is still controversially discussed. In flow reactor experiments, we found increased SOA formation from α-pinene ozonolysis in the presence of acidic, iron-containing droplets underlining the strong influence of pH and iron chemistry on SOA formation in multiphase systems.

1 Introduction

Secondary organic aerosol (SOA) plays an important role in the Earth's radiation budget by scattering and absorbing solar radiation, and by contributing to the number of cloud condensation nuclei.[1,2] After gas-phase oxidation of volatile organic compounds (VOCs) and subsequent gas-to-particle conversion of semi-volatile compounds, SOA particles grow and chemically age in the atmosphere. With lifetimes from hours to weeks, SOA is considered a short-lived climate-forcer.[3]

To predict SOA properties and behavior in the atmosphere, a comprehensive understanding of formation pathways is crucial. Extremely-low volatile organic compounds (ELVOC) and highly oxygenated molecules (HOM) play an important role in the formation and growth of SOA.[4,5] In particular, oxidation products of monoterpenes ($C_{10}H_{16}$) contribute significantly to global SOA formation. One of the most abundant natural monoterpenes, α-pinene, has been extensively studied,[6–8] and together with ozone (O_3) it is an important SOA-forming system in the troposphere.[8–11] Major products include highly oxidized carboxylic acids and dimers.[7] Field studies also showed that SOA from α-pinene ozonolysis can contribute significantly to the organic content in cloud water.[12] Previous studies on dimer esters of α-pinene SOA have found higher concentrations of dimers during night time.[7,13] As an explanation, some studies suggested the limited formation of α-pinene Criegee intermediates and dimers due to high OH concentrations during daytime.[14]

[a]*Environmental Chemistry and Air Research, Technische Universität Berlin, 10623 Berlin, Germany. E-mail: sabine.luechtrath@tu-berlin.de*

[b]*Univ Lyon, Université Claude Bernard Lyon 1, CNRS, IRCELYON, F-69626, Villeurbanne, France*

† Electronic supplementary information (ESI) available. See DOI: https://doi.org/10.1039/d4ea00095a

‡ Current laboratory: Department of Chemistry, Aarhus University, 8000 Aarhus, Denmark.

During night time, main atmospheric oxidants are O_3 in the gas-phase and OH radicals in the aqueous phase. However, large uncertainty persists about the source of OH radicals in cloud droplets. One important and frequently discussed pathway is the Fenton reaction, which leads to the oxidation of organic compounds by the formation of OH radicals.[15,16] In the absence of sun light and under acidic conditions the chain reaction can be summarized by reaction (1):[17]

$$Fe^{2+} + H_2O_2 + H^+ \rightarrow Fe^{3+} + HO^{\bullet} + H_2O \quad (1)$$

The presence of H^+ is required to enable the decomposition of H_2O_2. To achieve the maximum amount of OH radicals, pH levels near 3 are reported to be the optimum.[18–21]

Fenton's reaction is driven by iron, the most abundant transition metal of the earth's crust. The main source of atmospheric iron is wind erosion. In addition, anthropogenic sources such as traffic, combustion and industrial processes can lead to iron emissions especially in urban areas. Depending on anthropogenic activity and natural erosion events dissolved iron concentrations in fog and cloud water can vary considerably, ranging between 0.02 and 647 μmol L^{-1}.[16,22]

Hydrogen peroxide is omnipresent in atmospheric waters and reaches concentrations of levels up to 100 μmol L^{-1} in cloud and fog water.[23] In aqueous mixtures of iron and SOA, the influence of SOA on Fenton chemistry is still controversially discussed. Several studies suggest that the decomposition of SOA through Fenton's reaction leads to an enhanced formation of OH radicals in the dark and under UV light.[24,25] Contrary to that, other studies suggest that SOA suppresses the production of OH radicals in the presence of UV light.[26] Moreover, carboxyl functional groups can form complexes with iron, thus inhibiting the decomposition of organic material in the aqueous phase.[27] If generated *via* Fenton's reaction, OH radicals can increase chemical aging of SOA by facilitating fragmentation, functionalization and oligomerization.[28–30] Thus, the presence of iron can either enhance or inhibit the formation and growth of SOA particles. This study attempts to investigate the impact of water-soluble iron on formation and transformation of SOA under dark, humid and varying pH conditions in the presence and absence of H_2O_2.

2 Material and methods

2.1 General experimental design

The influence of the aqueous-phase iron chemistry on SOA formation by α-pinene ozonolysis was investigated by using a flow tube reactor (Fig. 1) in the presence of aqueous droplets and under controlled aerosol/gas-phase conditions. In total 31 flow reactor experiments were conducted in four experiment sets under varying conditions of aqueous droplet composition, pH, O_3 concentration, reaction time and relative humidity (RH) (see Tables 1 and S1†).

In the flow tube reactor, gaseous α-pinene and O_3 were mixed with aqueous droplets of different concentrations of $FeSO_4$ (FS) or $(NH_4)_2SO_4$ (AS). AS was used in iron-free control experiments. Ozonolysis of α-pinene leads to the formation of oxidation

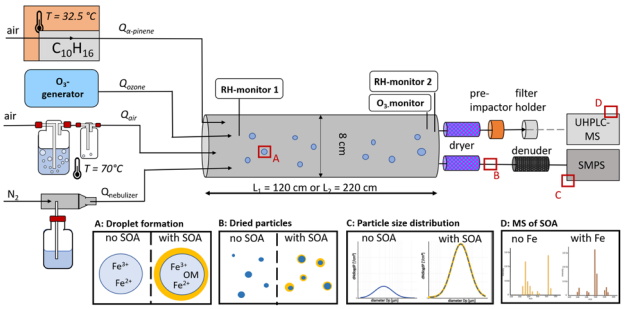

Fig. 1 Summary of experimental set-up and schematic representation of observations.

products with vapor pressures sufficiently low to condense onto aerosol particles[31] or droplets. Droplets were dried at the outlet of the flow tube. Due to typical oxygen-to-carbon ratios O : C < 0.8, liquid–liquid separation is likely to take place during the drying process.[32,33] Variations in the resulting particle size distributions of dried droplets were measured with a scanning mobility particle sizer (SMPS, Grimm Aerosoltechnik, Ainring, Germany), and organic marker compounds in aerosol samples were analyzed by liquid chromatography coupled to high-resolution mass spectrometry (UHPLC-HESI-Orbitrap-MS). All experiments were conducted in the dark thus preventing photochemical reactions, and under humid conditions (relative humidity RH > 60%) avoiding recrystallization of dissolved salts.

Table 1 summarizes all experimental conditions. In the following, the flow reactor, the experimental procedures and the analytical equipment including data analysis are described in detail.

2.2 Flow reactor

Standardized metal pipes with a diameter of 80 mm and lengths of either 100 cm or 200 cm were installed between two end caps with a volume of 0.5 L each, resulting in an opaque reaction volume (V_r) of 6 L and 11 L, respectively. Each end cap was equipped with a relative humidity sensor (RH1 & RH2) (BME 280, Bosch Sensortec, Reutlingen, Germany). The inlet end cap contained four inlets for humidified air, the reactant gas, the oxidant gas, and droplets. RH in the flow reactor was adjusted by leading a purified air stream through warm water of 70 °C and a droplet trap at a volume flow rate of 1.5 L min^{-1} (Table 1, sets 1 and 2) and 3.5 L min^{-1} (Table 1, sets 3 and 4). The humidified air stream was cooled down before entering the flow reactor leading to temperatures in the flow tube between 19 °C and 23 °C. α-Pinene (≥98% Carl Roth GmbH & Co. KG, Karlsruhe, Germany) was introduced into a flow of purified air at 32.5 °C in a custom-built evaporator. A three-way valve either to pass the purified air stream through the evaporator at a volume flow rate of 0.5 L min^{-1} (Table 1, sets 1 & 2) or 0.2 L min^{-1} (Table 1, sets 3 & 4) or to bypass the evaporator was used to add α-pinene without changing the volume flow rate within the system. The average α-pinene concentration was calculated gravimetrically from the weight loss of liquid α-pinene in the

Table 1 Overview of all conducted experiments

	Parameters of nebulized solutions			Flow tube conditions								
	Salt	C_{salt} [mmol L^{-1}]	pH	C_{ozone} [ppb]	c_{aP} [ppm]	V_r [L]	ν [L min^{-1}]	t_r [s]	RH_1 [%]	RH_2 [%]	SOA formation	Repetition
1A	FS	0.0001–10	4–6	435	1.8–2.5	6	6.7	50	>60	>70	Yes	3
1B	AS	0.0001–10		435	1.8–2.5	6	6.7	50	>60	>70	Yes	3
1C	FS	0.0001–10	4–6	0	0	6	6.7	50	>60	>70	No	2
1D	AS	0.0001–10		0	0	6	6.7	50	>60	>70	No	2
2A	FS	0.001; 0.1	≈5.5	435	1.8–2.5	6	6.7	50	>60	>70	Yes	5
2B	AS	0.001; 0.1		435	1.8–2.5	6	6.7	50	>60	>70	Yes	3
3A	FS	0.1 ($\pm H_2O_2$)	<3 & 5.5	485	3.0–4.3	11	6	110	>90	>90	Yes	2
3B	FS	0.1 ($\pm H_2O_2$)	<3 & 5.5	195	3.0–4.3	11	6	110	>90	>90	Yes	3
4	FS	0.1 ($\pm H_2O_2$)	<3 & 5.5	195	3.0–4.3	11	6	110	>90	>90	Yes	2

evaporator before and after the experiment. Ozone was generated by an ozone generator (2B Technologies Model 306, Boulder, CO, USA) and introduced into the system at a volume flow rate of 2.9 L min^{-1} (experiment sets 1 & 2) or 0.5 L min^{-1} (experiment sets 3 & 4). Ozone mixing ratios were monitored by ultraviolet absorption (Model APOA360, HORIBA Ltd, Kyōto, Japan).

Droplets were generated by nebulizing aqueous salt solutions of different composition and concentration with nitrogen gas by a custom-built atomizer constructed according to a protocol published elsewhere.[34] Droplets were constantly introduced into the system directly without drying at a volume flow rate of 1.8 L min^{-1}. The total volume flow rate in the flow reactor was 6.7 L min^{-1} (Table 1, sets 1 & 2) and 6 L min^{-1} (Table 1, sets 3 & 4), resulting in average residence times of 50 s and 110 s, respectively. The outlet flow was dried by a silica gel diffusion dryer, and reactive gases were removed with an activated charcoal denuder before particles were counted, size-classified, or collected. All tubing and fitting material was made of Teflon or stainless steel. To prevent photochemical reactions within the system, only brown glass vessels were used and all tubes were darkened by aluminium foil and duct tape.

2.3 Experimental procedures

The first set of experiments (1A–1D) was designed to investigate the change of particle size distributions in the presence of aqueous droplets with varying concentrations of FS and AS salts at RH ≥ 60%. RH was above the efflorescence RH of pure AS ranging from 31 to 48%.[35] Solutions of FS ($Fe(II)SO_4$, ≥95%, Carl Roth, Karlsruhe, Germany) and AS ($(NH_4)_2SO_4$, Merck, Darmstadt, Germany) were prepared before each experiment with bi-distilled water in the range of 0.0001–10 mmol L^{-1}. For each concentration, experiments in the presence of α-pinene and ozone were repeated three times, and twice in the absence of α-pinene and ozone. pH values of the iron-containing solution varied depending on the salt concentration between 2.7 and 6 (see Table 1). For each experiment, after the equilibrium conditions were reached in the flow tube reactor, at least five consecutive SMPS scans, *i.e.* 20 min of particle size distribution measurements of the dried droplets were made. The experiments were carried out in order of the solutions' concentration to prevent carryover of ions. Between each experiment, the flow reactor was thoroughly washed and flushed with excess O_3 to remove organic residues of α-pinene and its oxidation products. Memory effects were not observed.

The second set of experiments (2A & 2B) was conducted to systematically investigate α-pinene SOA formation in the presence and absence of ferrous iron in droplets. The size distributions comparison between pure salt particles and size distributions after SOA formation enables a direct calculation of newly formed SOA. In the second set of experiments, 0.001 and 0.1 mmol L^{-1} solutions of FS and AS were prepared with bi-distilled water and nebulized. Salt concentrations were selected based on the results of the first experiment set. Control experiments with AS and the investigated experiments with FS were repeated 3 and 5 times for each concentration, respectively.

The third set of experiments (3A & 3B) was conducted similarly to experiments 2A and 2B but with an emphasis on varying pH and H_2O_2 concentrations favouring Fenton's reaction in the droplets.[36] FS solution of 0.1 mmol L^{-1} was systematically acidified by gently adding 32% HCl (AnalaR NORMAPUR, VWR Germany, Darmstadt, Germany) until a pH < 3 was reached and/or spiked with 30% H_2O_2 (ROTIPURAN, Carl Roth GmbH + Co. KG, Karlsruhe, Germany) to reach a concentration of 1 mmol L^{-1}. The presence or absence of H_2O_2 and HCl leads to four different combinations of solutions shown in Table S1.† Solution I was pure 0.1 mM FS solution. For solution II, H_2O_2 was added. In solutions I and II, Fenton chemistry was not expected to be effective because of rather high pH conditions (pH was approximately 5.5). Solutions III and IV were acidified with HCl (pH < 3), and solution IV also contained H_2O_2. If OH radicals are produced by Fenton chemistry within the droplet, oxidation of water-soluble SOA or water soluble SVOCs can be expected. Thus, the strongest OH production was expected to take place in the droplets generated from solution IV.

Finally, the fourth set of experiments was a replicate of experiment 3B for sample collection onto filters but all solutions were prepared using HPLC-MS grade water. Experiments nebulizing pure HPLC-MS grade water were used as control

experiments. The outflow was dried and led through a custom-built pre-impactor removing particles >250 nm. The remaining particles were collected on 47 mm quartz fiber filters (Munktell MK360, Ahlstrom Munksjö, Helsinki, Finland) with a stainless-steel inline filter holder at a flow rate of 5 L min^{-1} for 10 h. Each of the four solutions and the reference solution were nebulized twice to get duplicates resulting in 10 filter samples.

2.4 Analytical procedure

2.4.1 Physical analysis. In experiments 1–3, particle size distributions within the diameter range of 5 to 350 nm were measured using an SMPS. When SOA formation was active an organic-rich coating was expected to develop on the droplets. Those droplets were dried which resulted either in a population of pure inorganic salt particles or a population of mixed salt particles with SOA coating. An average size distribution was constructed from three stable size distribution scans, and subsequently log-normally fitted by using the smps.py python package (QuantAQ, Inc., 2023). For data averaging, a minimum deviation criterion of the total number concentration (TNC) was applied to select three SMPS scans under stable conditions in the flow reactor. The largest deviation of TNC between three scans was 11.5%. Based on the log normal size distribution, geometric mean diameter (GMD), surface area (A) and volume concentration (V) were calculated for both the salt and mixed particles. The mass concentration of condensed SOA was estimated by calculating the difference in total mass concentration (ΔTMC) between pure salt particles and mixed particles. For volume-to-mass conversion a density of the condensed organic material of 1 g cm^{-3} was assumed.

2.4.2 Chemical analysis. Filter samples were extracted in slightly alkaline conditions and extracted by solid phase extraction (SPE) C18 cartridges (100 mg mL^{-1}, CHROMABOND, Macherey-Nagel GmbH& Co KG, Düren, Germany) following the procedure of Schmitt-Kopplin *et al.* (2010)[37] described in detail in the ESI.† For subsequent chemical analysis, ultra-high performance liquid chromatography (UHPLC, Dionex 3000, Thermo Scientific, USA) coupled with a diode array detector (DAD, Dionex UltiMate3000, Thermo Scientific, USA) and an Orbitrap high-resolution mass spectrometer (HRMS, Q Exactive, Thermo Scientific, Bremen, Germany) using heated electrospray ionization (HESI) was used. 5 μL of the sample were injected and analytes were separated using a Waters Acquity HSS T3 column (1.8 μm, 100 × 2.1 mm). Gradient and instrument settings are described elsewhere.[38] Each duplicate was measured in negative HESI mode. To quantify contamination, blanks of the flow tube system and the SPE procedure were taken and analyzed. The chromatogram-mass spectra were analyzed by Xcalibur4.1 (Thermo Scientific, USA). Target peak and structure identification was based on literature (see Table S2†). Camphorsulfonic acid (CSA) was used as internal standard to check the injection. Interestingly, after analysis the CSA signal decreased for all samples containing SOA from α-pinene ozonolysis by at least 12% while all blank and pure water samples did not show a significant decrease of the CSA concentration. It can be assumed that the injection was performed correctly but that some matrix effects of the different samples had impacts on the CSA concentration. For this reason, the signal was not corrected and results are shown without any normalization. Lack of normalization may lead to some uncertainty in peak interpretation.

3 Results and discussion

In the first set of experiments, size distributions in experiments with SOA formation *via* α-pinene ozonolysis (1A&1B) were compared to particle size distributions in experiments when neither α-pinene nor ozone were introduced into the system (1C&1D). Fig. 2 shows size distributions and the GMD across the whole concentration range for FS and AS particles in the presence and absence of SOA formation. For both FS and AS, higher ion concentrations lead to an increase in TNC of the pure salt particle population and a slight increase in GMD when concentrations exceed 1 mmol L^{-1} (in the absence of α-pinene ozonolysis, solid lines). In the presence of α-pinene ozonolysis, a strong increase in TNC and a decrease of GMD of the mixed particle population (broken lines) is observed compared to the pure salt particle population. Moreover, the increase in TNC and reduction in GMD of the mixed particle population is stronger with increasing salt concentrations. Furthermore, the unimodal particle size distribution observed in the presence of α-pinene ozonolysis indicated internally mixed SOA particles. We assume that an increase in salt concentration is likely to not only lead to increased droplet formation (and thus an increase of the pre-existing droplet surface area) but also to an increase in ion concentration of each droplet and, thus, an increase in ionic strength. When gas-phase α-pinene ozonolysis is initiated, α-pinene is oxidized to less volatile and more polar compounds which increases their water solubility. The partitioning of a compound between the gas-phase and the aqueous phase can

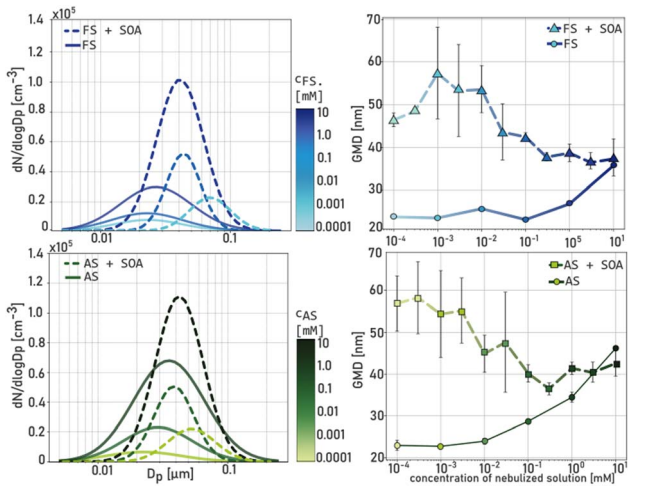

Fig. 2 Change of size distribution (1A and 2A) and GMD (1B and 2B) with increasing salt concentrations. The solid lines represent particle size distribution and GMD of pure salt particles (FS in blue, AS in green). The dashed lines represent particle size distributions and GMD of mixed particle populations of salt and SOA.

be described by Henry's law at thermodynamic equilibrium. Henry's law is only applicable for dilute solutions and equilibrium adjustment may not be instantaneous for example due to kinetic limitations.[32] For concentrated solutions, chemical composition and ionic strength of the electrolytes leading to "salting in" and "salting out" effects have to be considered.[39] One study determined Henry coefficients (air/water) for 14 α-pinene oxidation products revealing an increase of Henry coefficients by one to two orders of magnitude in the presence of 4 M AS solution.[40] Overall, higher ion concentrations in the droplets seem to inhibit organic particle growth. To quantify newly formed particle number and mass, a second set of experiments was conducted where particle size distributions in the presence and absence of α-pinene ozonolysis were measured systematically within one experiment as described in Section 2.3. Similar to observations in the first set of experiments, an increase of AS and FS concentrations by two orders of magnitude from 0.001 to 0.1 mmol L^{-1} lead to an increase of TNC and to a decrease in GMD of the internally mixed particle population. The smaller GMD corresponds to a decrease in total particle surface area and to a decrease in total particle volume as visualized in Fig. 3. Surprisingly, the number of newly formed particles increased with higher AS and FS concentrations while the newly formed SOA mass decreased significantly with higher AS and FS concentrations. The ratio of newly formed SOA mass to surface area of pure salt particles, $\Delta TMC/A_{salt}$ significantly decreases with increasing seed surface area (and ion concentration) for both AS and FS (see Fig. S1†). There are no clear differences between the 0.001 mmol L^{-1} solutions and bi-distilled water. These findings imply that in this specific set of experiments, low concentrations of 0.001 mmol L^{-1} do not have a significant influence on SOA mass formation. As mentioned above, the increase of AS and FS concentration to 0.1 mmol L^{-1} in the nebulized solutions increases the ionic strength within the droplet which might affect the solubility of more water soluble multifunctional organic compounds. Pinic acid, for example, an LVOC formed *via* the oxidation of nonpolar α-pinene[41,42] has an estimated Henry's law constant of 1.02 × 10^7 M per atm and can thus partition into the aqueous phase where it can participate in processes like hydration or radical oxidation.[15,43] If the salting out effect due to ionic strength in the droplet solution reduces the transfer of LVOCs and especially SVOCs into the aqueous phase, these compounds are enriched in the gas-phase and facilitate nucleation of SOA. Nucleation could then compete with condensation on pre-existing particles, thus producing more small particles but inhibiting the growth of pre-existing particles as observed when increasing the ion concentration in the presence of α-pinene ozonolysis (Fig. 3). Previous studies demonstrated a decrease in ozone solubility with increasing ionic strength resulting in lower Henry-coefficients.[44,45] Besides, Mekic *et al.* (2018) observed an increased reactive uptake of ozone with rising ionic strength in the presence of pyruvic acid in the aqueous phase.[44] In the context of measurement accuracy at high relative humidity for the ozone monitor, minor fluctuations in ozone concentration are challenging to interpret.[46] Since no clear changes in ozone concentration with increasing ionic strength were observed the

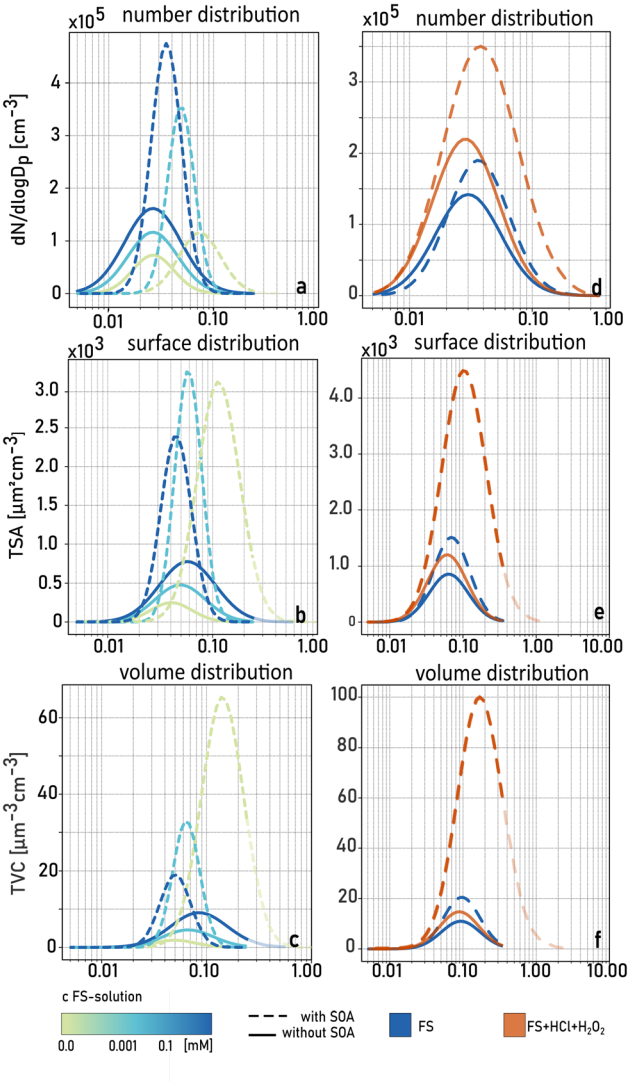

Fig. 3 Number (a), surface (b) and volume (c) size distribution when nebulizing bi-distilled water (yellow) or 0.001 mM (light blue) and 0.1 mM (dark blue) FS solution. Number (d), surface (e) and volume (f) size distributions when nebulizing solutions of category IV (FS, HCL, H_2O_2) in orange and category I (FS) in blue. Solid lines represent populations of pure salt particles. Dashed lines represent populations of mixed salt and SOA particles.

change of ozone solubility by 'salting out' effect is not considered as an important factor in the variation of SOA formation observed in the experiments. Moreover, particle size distributions did not change when α-pinene was introduced into the system without ozone.

Overall, the first two sets of experiments underline the influence of ions in the aqueous phase on SOA formation but do not show a specific influence of ferrous iron being present in the droplet.

The third set of experiments was designed to investigate whether chemical reactions involved in SOA formation can be affected by providing conditions favorable for Fenton chemistry, *i.e.* acidic conditions (pH < 3) and the presence of H_2O_2 in the aqueous droplets. The oxidation of Fe(II) *via* oxygen is very

slow – but the addition of H_2O_2 is expected to accelerate the oxidation of ferrous iron in the aqueous phase according to reaction (1) (Section 1). In the aqueous phase under dark conditions, the production of OH radicals by the oxidation of Fe(II) to Fe(III) is dependent on pH and H_2O_2 concentrations.[36]

Fig. 3 shows examples of number, surface, and volume size distributions of particle populations with (broken lines) and without (solid lines) SOA formation under acidic (pH < 3, red) and 'non-acidic' (pH > 3, blue) conditions. All calculated parameters are listed in Table S1.† Without SOA formation, the addition of HCl leads to a significant increase of particle number due to additional chloride salts but similar surface and volume size distributions compared to the 'non-acidic' experiments. In the presence of SOA formation, there is a strong increase in particle number, surface, and volume concentrations, and a broader size distribution under acidic conditions. This is also illustrated in a strong increase in total mass concentration due to SOA formation (TMC) under acidic conditions (Fig. 4, categories III & IV) compared to experiments when the FS solution was not acidified (Fig. 4, categories I & II). Table S1† summarizes TNC, TMC and GMD of all particle populations in the third set of experiments. As mentioned before, additional salt particles formed when adding HCl do not have a significant influence on the surface area of the pure salt particles (A_{salt}), and therefore, TMC/A_{salt} is strongly increased when the solution was acidified (category III & IV). A simultaneous increase in GMD indicates an intensified process of SOA condensation under acidic conditions.

Furthermore, an increase in the number of newly formed particles is observed under acidic conditions (category III & IV) compared to 'non-acidic' conditions. This finding suggests an additional oxidation pathway of α-pinene ozonolysis products. Across all experiments, the acidified solutions led to a slow but constant increase of TNC, TMC and GMD for salt particles with SOA formation (see Fig. S2†). While particle size distributions were stable within a few minutes when nebulizing 'non-acidic' AS and FS solutions with simultaneous SOA formation, it took more than an hour to reach stable conditions when nebulizing acidified FS solutions indicating a disturbed equilibrium by ongoing chemical reactions in the acidified bulk nebulizing solution. When comparing the results of categories III and IV, the presence of H_2O_2 in the FS solution did not have a clear effect on TNC or TMC. This result indicates that a low pH is crucial for the ongoing reactions in this set of experiments.

Considering reaction (1), the third set of experiments suggests that OH is formed by Fenton chemistry in FS droplets under acidic conditions at pH < 3. On the one hand, this can lead to further aqueous-phase oxidation of water soluble organic compounds by OH radicals eventually forming SOA,[47,48] which results in an increased GMD after drying. On the other hand, several studies reported the decomposition of SOA in the aqueous phase in the presence of Fe(II).[24,25,49] Therefore, water-soluble organic compounds can also be degraded to more volatile organic compounds which can be re-emitted into the gas-phase. These released compounds might undergo gas-phase oxidation for a second time.

Previous studies report that the presence of Cl^--ions in the aqueous phase can scavenge the OH radicals which were formed during Fenton's reaction according to eqn (2)–(4):[50]

$$OH + Cl^- \leftrightarrow ClOH^- \quad (2)$$

$$ClOH + H^+ \leftrightarrow Cl + H_2O \quad (3)$$

$$Cl + Cl^- \leftrightarrow Cl_2^- \quad (4)$$

Studies observed scavenging above 0.01 M HCl at pH 2.8.[51] In the nebulized solution the concentration of HCl was less than 10^{-3} mol L^{-1}. Therefore, we assume that the influence of OH-scavenging in the acidic samples might be low and thus also the oxidation by chlorine but the scavenging of O radicals and further oxidation by chlorine might be an important oxidation pathway in environments of high salinity.

Furthermore, aerosol acidity influences the reactive uptake and thus particle formation.[52,53] When present in the aqueous phase, carbonyl-containing compounds formed *via* α-pinene ozonolysis can undergo hydration which is catalyzed by acids and bases. Through hydration the carbonyl group is converted into gem-diol moieties. This increases the effective reactive uptake of carbonyl-containing compounds due to the hydration equilibrium.[54] Therefore, the addition of HCl might not only lead to the formation of OH radicals by Fenton-like chemistry but also increases the reactive uptake into the aqueous phase.

To elucidate the effect of Fenton chemistry and the role of acidity on the observed increased SOA mass, particles were finally collected in a fourth set of experiments when solutions of category I to IV were nebulized, separated by liquid chromatography, and analysed by high-resolution MS. In particular, the abundance of specific oxidation products of α-pinene ozonolysis was investigated to get a first impression of the dominant chemical reactions taking place in the aqueous phase. As a reference sample in addition to the four FS containing solutions (category I–IV), HPLC-MS grade water was nebulized and α-pinene SOA formation initiated. An overview of the main investigated compounds within the samples is listed in Table S2.† In the following, the reference sample will be compared with the sample of category IV representing conditions favoring Fenton chemistry. In all samples, pinonaldehyde ($C_{10}H_{16}O_2$),

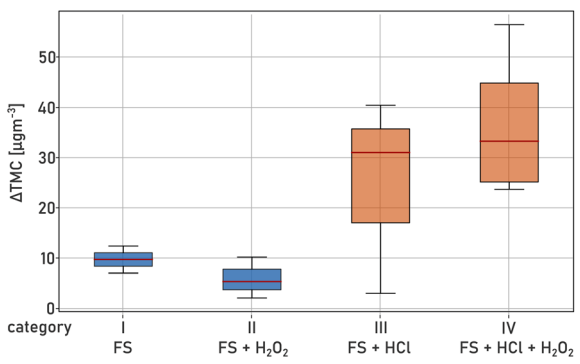

Fig. 4 Comparison of formed SOA mass under different conditions in the aqueous phase.

one of the major first-generation oxidation products of α-pinene ozonolysis,[55,56] gave the most abundant signal. Fig. 5 shows the relative abundance of selected extremely low-volatile compounds (ELVOC) including various dimers such as pinyl-diaterpenyl ester (MW 358) and pinonyl-pinyl ester (MW 368) in the duplicates of the reference sample (yellow) and the sample of category IV (red). The samples of category II and III are illustrated in Fig. S3.† Whereas most compounds were found in all samples, several compounds were found in much higher or lower concentration in the reference sample compared to the Fenton's chemistry sample of category IV. For example, pinyl-diaterpenyl ester $C_{17}H_{26}O_8$ (MW 358), a compound typical of early stage SOA formation,[57] showed high abundance in α-pinene SOA of the reference sample (Fig. 5, yellow) and much lower abundance in samples of category IV (Fig. 5, red) with active Fenton's chemistry. In contrast, a high abundance of the dimer $C_{19}H_{30}O_5$ (MW 338), which has been suggested to be an accretion product by aldol reaction of *cis*-pinonic acid and pinonaldehyde or norpinonaldehyde,[57,58] was found in the samples with active Fenton's chemistry (Fig. 5, red) but only in lower abundance in the reference sample (Fig. 5, yellow). Pinyl-diaterpenyl ester has been reported as a dimer of α-pinene ozonolysis in previous studies.[14,58–60] Some studies investigated the aging of pinyl-diaterpenyl ester by aqueous OH oxidation.[59] They estimated the aqueous decay of pinyl-diaterpenyl ester and proposed fragmentation to monomeric products, which are suggested to be volatile and thus re-emitted into the air[61] where they can undergo further gas-phase oxidation leading to new particle formation. The significantly lower abundance of pinyl-diaterpenyl ester in the Fenton's chemistry sample in our study is consistent with the expected OH production in the droplet.

However, in a study using lower Fe(II) concentrations a decrease in OH production in the presence of α-pinene SOA was found[26] indicating that the concentration ratio between Fe(II) and water-soluble organic compounds is crucial for OH production. The lower abundance of pinyl-diaterpenyl ester in the acidified sample of category III further implies the pH dependency of iron chemistry leading either to the formation of OH radicals *via* Fenton-like chemistry or other acidity-driven reactions.

Anyway, the decomposition of dimers like pinyl-diaterpenyl ester or pinonyl-pinyl ester through OH oxidation are not strongly dependent on pH,[59,60] while the aldol reaction forming dimer MW 338 is suggested to be acid-catalyzed. The pronounced abundance of dimer MW 338 in the Fenton's chemistry samples of category IV but also in the acidified sample of category III in our study suggests that at least two major mechanisms of SOA transformation are taking place simultaneously, *i.e.*:

(1) Iron related processes and especially Fenton's chemistry leading to the decomposition of high-molecular weight SOA by OH production and aqueous phase oxidation and (2) acid-catalyzed formation of high-molecular weight SOA in the aqueous phase. Previous studies report a decrease in SOA growth and inhibition of SOA formation in the presence of Fe(II) under humid conditions and in the presence of sunlight when OH production is expected to be increased compared to dark conditions.[29,62] Consistent with our results, they suggest a decomposition of SOA through OH oxidation and a subsequent evaporation into the gas-phase. In the presence of sunlight, gas-phase oxidation of α-pinene by OH radicals is favored to take place which does not lead to the formation of high-molecular weight dimers.[14] Furthermore, dimers like dimer MW 338 can be photolyzed,[63] and thus, the irradiation of aqueous-phase SOA may also lead to a reduction in molecular mass.[64] Therefore, a possible explanation for the contrasting results of the influence of Fenton's chemistry on SOA formation discussed in the literature could be that photo-chemical processing of SOA masks the reaction with aqueous-phase OH oxidation during photo-Fenton's reaction.

A typical marker of gas-phase OH oxidation of pinonaldehyde and *cis*-pinonic acid is 3-methyl-1,2,3-butanetricarboxylic acid (MBTCA).[14,41,65–67] In all samples, MBTCA was not detected underlining that gas-phase OH oxidation in the flow reactor did not contribute considerably to SOA mass.

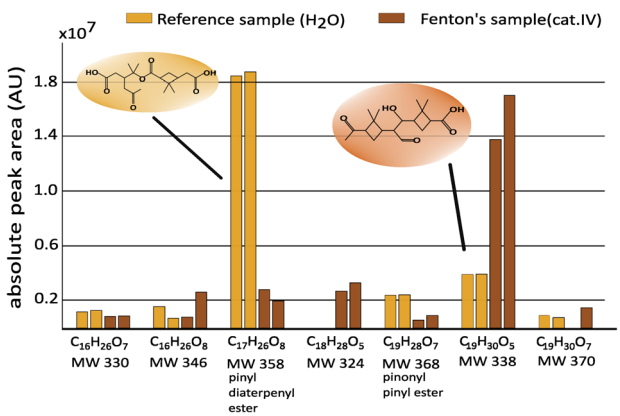

Fig. 5 Relative abundance of selected ELVOC in duplicates of samples collected under conditions favouring Fenton's chemistry (red) and in reference samples (yellow).

4 Conclusions

The role of atmospheric soluble iron in the formation and fate of SOA is a controversial topic. In atmospheric waters, soluble iron can reach concentration levels of several hundred μmol L^{-1}. Depending on sources and environmental conditions iron solubility varies considerably. While iron from mineral-dust contributes only 1% to the water-soluble iron fraction, pyrogenic iron mostly contributes a larger fraction of water soluble iron.[68,69] Therefore, the concentration of water-soluble iron in atmospheric waters varies locally over several orders of magnitude.[22] Moreover, atmospheric waters vary significantly in pH. For example, pH in cloud waters ranges from 2–7.[70] In our experiments we observed an increase in SOA formation in acidic aqueous mixtures of SOA, ferrous iron and H_2O_2 indicating that iron and/or acidity related processes increase SOA formation in the aqueous phase. Iron chemistry is complex and depending on various parameters such as oxidation state, presents ligands and the pH. By offline high-resolution mass spectrometry we

found lower abundance of pinyl-diaterpenyl ester in the acidic aqueous mixtures of SOA, ferrous iron and H_2O_2 compared to reference samples of aqueous SOA. This finding indicates a decomposition of SOA by radicals formed *via* iron chemistry and most likely Fenton's chemistry. Moreover, we found a decrease in dimer MW 338 in the acidic samples indicating acidity driven dimer formation. These findings give us a hint of various processes ongoing simultaneously in the aqueous phase.

Even though the offline chemical characterization of our filter samples is not sufficient to elucidate a major reaction pathway, which would fully explain the increased SOA mass under conditions favouring Fenton chemistry, this study highlights some of the challenges of estimating the influence of water-soluble iron chemistry on SOA formation and transformation. Our experiments outline the complexity and pH dependency of iron chemistry and its influence on various processes in atmospheric waters. This emphasizes the crucial interaction between practical laboratory experiments and theoretical modelling for a comprehensive understanding of iron-related processes in these environments. Consequently, further research on iron chemistry under naturally relevant conditions and varying pH is essential, both in laboratory experiments and modelling, to elucidate all processes taking place in the aqueous phase.

Data availability

The data supporting this article have been included as part of the ESI.† All raw data used for this article, including SMPS- and HPLC-Orbitrap-MS-data are available at zenodo [**https://zenodo.org/doi/10.5281/zenodo.12582477**].

Author contributions

SL: conceptualization, data curation, formal analysis, investigation, methodology, visualization, writing – original draft; SK: conceptualization, methodology; CD: conceptualization, methodology, writing – review & editing; CG: conceptualization, resources, writing – review & editing; AH: conceptualization, resources, supervision, validation, writing – review & editing.

Conflicts of interest

There are no conflicts to declare.

Acknowledgements

Special thanks to Max Zeidler for the construction of the atomizer.

Notes and references

1 T. Yli-Juuti, T. Mielonen, L. Heikkinen, A. Arola, M. Ehn, S. Isokääntä, H.-M. Keskinen, M. Kulmala, A. Laakso, A. Lipponen, K. Luoma, S. Mikkonen, T. Nieminen, P. Paasonen, T. Petäjä, S. Romakkaniemi, J. Tonttila, H. Kokkola and A. Virtanen, Significance of the organic aerosol driven climate feedback in the boreal area, *Nat. Commun.*, 2021, **12**, 5637.

2 T. Drugé, P. Nabat, M. Mallet, M. Michou, S. Rémy and O. Dubovik, Modeling radiative and climatic effects of brown carbon aerosols with the ARPEGE-Climat global climate model, *Atmos. Chem. Phys.*, 2022, **22**, 12167–12205.

3 S. Dhakal, J. C. Minx, F. L. Toth and Y. Shan, in *Climate Change 2022: Mitigation of Climate Change: Contribution of Working Group III to the Sixth Assessment Report of the Intergovernmental Panel on Climate Change*, Cambridge University Press, 2022, pp. 215–275.

4 M. Ehn, J. A. Thornton, E. Kleist, M. Sipilä, H. Junninen, I. Pullinen, M. Springer, F. Rubach, R. Tillmann, B. Lee, F. Lopez-Hilfiker, S. Andres, I.-H. Acir, M. Rissanen, T. Jokinen, S. Schobesberger, J. Kangasluoma, J. Kontkanen, T. Nieminen, T. Kurtén, L. B. Nielsen, S. Jørgensen, H. G. Kjaergaard, M. Canagaratna, M. D. Maso, T. Berndt, T. Petäjä, A. Wahner, V.-M. Kerminen, M. Kulmala, D. R. Worsnop, J. Wildt and T. F. Mentel, A large source of low-volatility secondary organic aerosol, *Nature*, 2014, **506**, 476–479.

5 M. Riva, Multiphase Chemistry of Highly Oxidized Molecules: The Case of Organic Hydroperoxides, *Chem*, 2016, **1**, 526–528.

6 J. H. Seinfeld, G. B. Erdakos, W. E. Asher and J. F. Pankow, Modeling the Formation of Secondary Organic Aerosol (SOA). 2. The Predicted Effects of Relative Humidity on Aerosol Formation in the α-Pinene-, β-Pinene-, Sabinene-, Δ^3-Carene-, and Cyclohexene-Ozone Systems, *Environ. Sci. Technol.*, 2001, **35**, 1806–1817.

7 K. Kristensen, Å. K. Watne, J. Hammes, A. Lutz, T. Petäjä, M. Hallquist, M. Bilde and M. Glasius, High-Molecular Weight Dimer Esters Are Major Products in Aerosols from α-Pinene Ozonolysis and the Boreal Forest, *Environ. Sci. Technol. Lett.*, 2016, **3**, 280–285.

8 H. Zhang, L. D. Yee, B. H. Lee, M. P. Curtis, D. R. Worton, G. Isaacman-VanWertz, J. H. Offenberg, M. Lewandowski, T. E. Kleindienst, M. R. Beaver, A. L. Holder, W. A. Lonneman, K. S. Docherty, M. Jaoui, H. O. T. Pye, W. Hu, D. A. Day, P. Campuzano-Jost, J. L. Jimenez, H. Guo, R. J. Weber, J. De Gouw, A. R. Koss, E. S. Edgerton, W. Brune, C. Mohr, F. D. Lopez-Hilfiker, A. Lutz, N. M. Kreisberg, S. R. Spielman, S. V. Hering, K. R. Wilson, J. A. Thornton and A. H. Goldstein, Monoterpenes are the largest source of summertime organic aerosol in the southeastern United States, *Proc. Natl. Acad. Sci. U. S. A.*, 2018, **115**, 2038–2043.

9 R. Atkinson and J. Arey, Atmospheric Degradation of Volatile Organic Compounds, *Chem. Rev.*, 2003, **103**, 4605–4638.

10 K. S. Docherty, W. Wu, Y. B. Lim and P. J. Ziemann, Contributions of Organic Peroxides to Secondary Aerosol Formed from Reactions of Monoterpenes with O_3, *Environ. Sci. Technol.*, 2005, **39**, 4049–4059.

11 H. O. T. Pye, A. W. H. Chan, M. P. Barkley and J. H. Seinfeld, Global modeling of organic aerosol: the importance of

reactive nitrogen (NOx and NO3), *Atmos. Chem. Phys.*, 2010, **10**, 11261–11276.

12 Y. Zhao, A. G. Hallar and L. R. Mazzoleni, Atmospheric organic matter in clouds: exact masses and molecular formula identification using ultrahigh-resolution FT-ICR mass spectrometry, *Atmos. Chem. Phys.*, 2013, **13**, 12343–12362.

13 F. Yasmeen, R. Vermeylen, R. Szmigielski, Y. Iinuma, O. Böge, H. Herrmann, W. Maenhaut and M. Claeys, Terpenylic acid and related compounds: precursors for dimers in secondary organic aerosol from the ozonolysis of α- and β-pinene, *Atmos. Chem. Phys.*, 2010, **10**, 9383–9392.

14 K. Kristensen, T. Cui, H. Zhang, A. Gold, M. Glasius and J. D. Surratt, Dimers in α-pinene secondary organic aerosol: effect of hydroxyl radical, ozone, relative humidity and aerosol acidity, *Atmos. Chem. Phys.*, 2014, **14**, 4201–4218.

15 H. Herrmann, T. Schaefer, A. Tilgner, S. A. Styler, C. Weller, M. Teich and T. Otto, Tropospheric Aqueous-Phase Chemistry: Kinetics, Mechanisms, and Its Coupling to a Changing Gas Phase, *Chem. Rev.*, 2015, **115**, 4259–4334.

16 A. Bianco, M. Passananti, M. Brigante and G. Mailhot, Photochemistry of the Cloud Aqueous Phase: A Review, *Molecules*, 2020, **25**, 423.

17 L. Sigg and W. Stumm, *Aquatic Chemistry, Aquatische Chemie; Eine Einfuehrung in die Chemie waessriger Loesungen und natuerlicher Gewaesser*, 3rd edn, 1994.

18 S. M. Arnold, W. J. Hickey and R. F. Harris, Degradation of Atrazine by Fenton's Reagent: Condition Optimization and Product Quantification, *Environ. Sci. Technol.*, 1995, **29**, 2083–2089.

19 F. J. Rivas, F. J. Beltrán, J. Frades and P. Buxeda, Oxidation of *p*-hydroxybenzoic acid by Fenton's reagent, *Water Res.*, 2001, **35**, 387–396.

20 M. L. Kremer, The Fenton Reaction. Dependence of the Rate on pH, *J. Phys. Chem. A*, 2003, **107**, 1734–1741.

21 A. D. Bokare and W. Choi, Review of iron-free Fenton-like systems for activating H2O2 in advanced oxidation processes, *J. Hazard. Mater.*, 2014, **275**, 121–135.

22 L. Deguillaume, M. Leriche, K. Desboeufs, G. Mailhot, C. George and N. Chaumerliac, Transition Metals in Atmospheric Liquid Phases: Sources, Reactivity, and Sensitive Parameters, *Chem. Rev.*, 2005, **105**, 3388–3431.

23 A. V. Jackson and C. N. Hewitt, Hydrogen peroxide and organic hydroperoxide concentrations in air in a eucalyptus forest in central Portugal, *Atmos. Environ.*, 1996, **30**, 819–830.

24 H. Tong, A. M. Arangio, P. S. J. Lakey, T. Berkemeier, F. Liu, C. J. Kampf, W. H. Brune, U. Pöschl and M. Shiraiwa, Hydroxyl radicals from secondary organic aerosol decomposition in water, *Atmos. Chem. Phys.*, 2016, **16**, 1761–1771.

25 H. Tong, P. S. J. Lakey, A. M. Arangio, J. Socorro, C. J. Kampf, T. Berkemeier, W. H. Brune, U. Pöschl and M. Shiraiwa, Reactive oxygen species formed in aqueous mixtures of secondary organic aerosols and mineral dust influencing cloud chemistry and public health in the Anthropocene, *Faraday Discuss.*, 2017, **200**, 251–270.

26 R. F. Hems, J. S. Hsieh, M. A. Slodki, S. Zhou and J. P. D. Abbatt, Suppression of OH Generation from the Photo-Fenton Reaction in the Presence of α-Pinene Secondary Organic Aerosol Material, *Environ. Sci. Technol. Lett.*, 2017, **4**, 439–443.

27 J. Ma, W. Ma, W. Song, C. Chen, Y. Tang, J. Zhao, Y. Huang, Y. Xu and L. Zang, Fenton Degradation of Organic Pollutants in the Presence of Low-Molecular-Weight Organic Acids: Cooperative Effect of Quinone and Visible Light, *Environ. Sci. Technol.*, 2006, **40**, 618–624.

28 B. Ervens, B. J. Turpin and R. J. Weber, Secondary organic aerosol formation in cloud droplets and aqueous particles (aqSOA): a review of laboratory, field and model studies, *Atmos. Chem. Phys.*, 2011, **11**, 11069–11102.

29 B. Chu, Y. Liu, J. Li, H. Takekawa, J. Liggio, S.-M. Li, J. Jiang, J. Hao and H. He, Decreasing effect and mechanism of FeSO4 seed particles on secondary organic aerosol in α-pinene photooxidation, *Environ. Pollut.*, 2014, **193**, 88–93.

30 B. Ervens, Modeling the Processing of Aerosol and Trace Gases in Clouds and Fogs, *Chem. Rev.*, 2015, **115**, 4157–4198.

31 M. Hallquist, J. C. Wenger, U. Baltensperger, Y. Rudich, D. Simpson, M. Claeys, J. Dommen, N. M. Donahue, C. George, A. H. Goldstein, J. F. Hamilton, H. Herrmann, T. Hoffmann, Y. Iinuma, M. Jang, M. E. Jenkin, J. L. Jimenez, A. Kiendler-Scharr, W. Maenhaut, G. McFiggans, T. F. Mentel, A. Monod, A. S. H. Prévôt, J. H. Seinfeld, J. D. Surratt, R. Szmigielski and J. Wildt, The formation, properties and impact of secondary organic aerosol: current and emerging issues, *Atmos. Chem. Phys.*, 2009, **9**, 5155–5236.

32 G. T. Drozd, J. L. Woo and V. F. McNeill, Self-limited uptake of α-pinene oxide to acidic aerosol: the effects of liquid–liquid phase separation and implications for the formation of secondary organic aerosol and organosulfates from epoxides, *Atmos. Chem. Phys.*, 2013, **13**, 8255–8263.

33 M. Arak Freedman, Phase separation in organic aerosol, *Chem. Soc. Rev.*, 2017, **46**, 7694–7705.

34 B. Y. Liu and K. W. Lee, An aerosol generator of high stability, *Am. Ind. Hyg. Assoc. J.*, 1975, **36**, 861–865.

35 V. G. Ciobanu, C. Marcolli, U. K. Krieger, A. Zuend and T. Peter, Efflorescence of Ammonium Sulfate and Coated Ammonium Sulfate Particles: Evidence for Surface Nucleation, *J. Phys. Chem. A*, 2010, **114**, 9486–9495.

36 M. L. Kremer, Mechanism of the Fenton reaction. Evidence for a new intermediate, *Phys. Chem. Chem. Phys.*, 1999, **1**, 3595–3605.

37 P. Schmitt-Kopplin, A. Gelencser, E. Dabek-Zlotorzynska, G. Kiss, N. Hertkorn, M. Harir, Y. Hong and I. Gebefügi, Analysis of the unresolved organic fraction in atmospheric aerosols with ultrahigh-resolution mass spectrometry and nuclear magnetic resonance spectroscopy: organosulfates as photochemical smog constituents, *Anal. Chem.*, 2010, **82**, 8017–8026.

38 X. Wang, N. Hayeck, M. Brüggemann, L. Yao, H. Chen, C. Zhang, C. Emmelin, J. Chen, C. George and L. Wang, Chemical characteristics of organic aerosols in Shanghai: A study by ultrahigh-performance liquid chromatography

coupled with Orbitrap mass spectrometry, *J. Geophys. Res.: Atmos.*, 2017, **122**, 11–703.
39 R. Sander, Modeling Atmospheric Chemistry: Interactions between Gas-Phase Species and Liquid Cloud/Aerosol Particles, *Surv. Geophys.*, 1999, **20**, 1–31.
40 C. Wang, Y. D. Lei, S. Endo and F. Wania, Measuring and Modeling the Salting-out Effect in Ammonium Sulfate Solutions, *Environ. Sci. Technol.*, 2014, **48**, 13238–13245.
41 F. Yasmeen, R. Szmigielski, R. Vermeylen, Y. Gómez-González, J. D. Surratt, A. W. H. Chan, J. H. Seinfeld, W. Maenhaut and M. Claeys, Mass spectrometric characterization of isomeric terpenoic acids from the oxidation of α-pinene, β-pinene, d-limonene, and Δ3-carene in fine forest aerosol, *J. Mass Spectrom.*, 2011, **46**, 425–442.
42 A. Mutzel, L. Poulain, T. Berndt, Y. Iinuma, M. Rodigast, O. Böge, S. Richters, G. Spindler, M. Sipilä, T. Jokinen, M. Kulmala and H. Herrmann, Highly Oxidized Multifunctional Organic Compounds Observed in Tropospheric Particles: A Field and Laboratory Study, *Environ. Sci. Technol.*, 2015, **49**, 7754–7761.
43 V. F. McNeill, Aqueous Organic Chemistry in the Atmosphere: Sources and Chemical Processing of Organic Aerosols, *Environ. Sci. Technol.*, 2015, **49**, 1237–1244.
44 M. Mekic, G. Loisel, W. Zhou, B. Jiang, D. Vione and S. Gligorovski, Ionic-Strength Effects on the Reactive Uptake of Ozone on Aqueous Pyruvic Acid: Implications for Air–Sea Ozone Deposition, *Environ. Sci. Technol.*, 2018, **52**, 12306–12315.
45 A. V. Levanov, O. Y. Isaikina, R. B. Gasanova and V. V. Lunin, Solubility of Ozone and Kinetics of Its Decomposition in Aqueous Chloride Solutions, *Ind. Eng. Chem. Res.*, 2018, **57**, 14355–14364.
46 K. L. Wilson and J. W. Birks, Mechanism and Elimination of a Water Vapor Interference in the Measurement of Ozone by UV Absorbance, *Environ. Sci. Technol.*, 2006, **40**, 6361–6367.
47 A. K. Y. Lee, P. Herckes, W. R. Leaitch, A. M. Macdonald and J. P. D. Abbatt, Aqueous OH oxidation of ambient organic aerosol and cloud water organics: Formation of highly oxidized products, *Geophys. Res. Lett.*, 2011, **38**, DOI: 10.1029/2011GL047439.
48 A. K. Y. Lee, K. L. Hayden, P. Herckes, W. R. Leaitch, J. Liggio, A. M. Macdonald and J. P. D. Abbatt, Characterization of aerosol and cloud water at a mountain site during WACS 2010: secondary organic aerosol formation through oxidative cloud processing, *Atmos. Chem. Phys.*, 2012, **12**, 7103–7116.
49 T. Fang, P. S. J. Lakey, J. C. Rivera-Rios, F. N. Keutsch and M. Shiraiwa, Aqueous-Phase Decomposition of Isoprene Hydroxy Hydroperoxide and Hydroxyl Radical Formation by Fenton-like Reactions with Iron Ions, *J. Phys. Chem. A*, 2020, **124**, 5230–5236.
50 G. G. Jayson, B. J. Parsons and A. J. Swallow, Some simple, highly reactive, inorganic chlorine derivatives in aqueous solution. Their formation using pulses of radiation and their role in the mechanism of the Fricke dosimeter, *J. Chem. Soc., Faraday Trans. 1*, 1973, **69**, 1597.
51 J. J. Pignatello, E. Oliveros and A. MacKay, Advanced Oxidation Processes for Organic Contaminant Destruction Based on the Fenton Reaction and Related Chemistry, *Crit. Rev. Environ. Sci. Technol.*, 2006, **36**, 1–84.
52 J. Liggio and S.-M. Li, Reactive uptake of pinonaldehyde on acidic aerosols, *J. Geophys. Res.: Atmos.*, 2006, **111**, DOI: 10.1029/2005JD006978.
53 Y. Zhang, Y. Chen, Z. Lei, N. E. Olson, M. Riva, A. R. Koss, Z. Zhang, A. Gold, J. T. Jayne, D. R. Worsnop, T. B. Onasch, J. H. Kroll, B. J. Turpin, A. P. Ault and J. D. Surratt, Joint Impacts of Acidity and Viscosity on the Formation of Secondary Organic Aerosol from Isoprene Epoxydiols (IEPOX) in Phase Separated Particles, *ACS Earth Space Chem.*, 2019, **3**, 2646–2658.
54 A. J. Sumner, J. L. Woo and V. F. McNeill, Model Analysis of Secondary Organic Aerosol Formation by Glyoxal in Laboratory Studies: The Case for Photoenhanced Chemistry, *Environ. Sci. Technol.*, 2014, **48**, 11919–11925.
55 D. Johnson and G. Marston, The gas-phase ozonolysis of unsaturated volatile organic compounds in the troposphere, *Chem. Soc. Rev.*, 2008, **37**, 699–716.
56 R. Tillmann, M. Hallquist, Å. M. Jonsson, A. Kiendler-Scharr, H. Saathoff, Y. Iinuma and Th. F. Mentel, Influence of relative humidity and temperature on the production of pinonaldehyde and OH radicals from the ozonolysis of α-pinene, *Atmos. Chem. Phys.*, 2010, **10**, 7057–7072.
57 B. Witkowski and T. Gierczak, Early stage composition of SOA produced by α-pinene/ozone reaction: α-Acyloxyhydroperoxy aldehydes and acidic dimers, *Atmos. Environ.*, 2014, **95**, 59–70.
58 B. Witkowski, M. al-Sharafi, K. Błaziak and T. Gierczak, Aging of α-Pinene Secondary Organic Aerosol by Hydroxyl Radicals in the Aqueous Phase: Kinetics and Products, *Environ. Sci. Technol.*, 2023, **57**, 6040–6051.
59 R. Zhao, D. Aljawhary, A. K. Y. Lee and J. P. D. Abbatt, Rapid Aqueous-Phase Photooxidation of Dimers in the α-Pinene Secondary Organic Aerosol, *Environ. Sci. Technol. Lett.*, 2017, **4**, 205–210.
60 J. V. Amorim, S. Wu, K. Klimchuk, C. Lau, F. J. Williams, Y. Huang and R. Zhao, pH Dependence of the OH Reactivity of Organic Acids in the Aqueous Phase, *Environ. Sci. Technol.*, 2020, **54**, 12484–12492.
61 S. Enami and Y. Sakamoto, OH-Radical Oxidation of Surface-Active cis-Pinonic Acid at the Air–Water Interface, *J. Phys. Chem. A*, 2016, **120**, 3578–3587.
62 K. A. Kamilli, J. Ofner, B. Lendl, P. Schmitt-Kopplin and A. Held, New particle formation above a simulated salt lake in aerosol chamber experiments, *Environ. Chem.*, 2015, **12**, 489–503.
63 A. L. Klodt, D. E. Romonosky, P. Lin, J. Laskin, A. Laskin and S. A. Nizkorodov, Aqueous Photochemistry of Secondary Organic Aerosol of α-Pinene and α-Humulene in the Presence of Hydrogen Peroxide or Inorganic Salts, *ACS Earth Space Chem.*, 2019, **3**, 2736–2746.
64 H. Lignell, S. A. Epstein, M. R. Marvin, D. Shemesh, B. Gerber and S. Nizkorodov, Experimental and Theoretical

Study of Aqueous cis-Pinonic Acid Photolysis, *J. Phys. Chem. A*, 2013, **117**, 12930–12945.

65 R. Szmigielski, J. D. Surratt, Y. Gómez-González, P. Van der Veken, I. Kourtchev, R. Vermeylen, F. Blockhuys, M. Jaoui, T. E. Kleindienst, M. Lewandowski, J. H. Offenberg, E. O. Edney, J. H. Seinfeld, W. Maenhaut and M. Claeys, 3-methyl-1,2,3-butanetricarboxylic acid: An atmospheric tracer for terpene secondary organic aerosol, *Geophys. Res. Lett.*, 2007, **34**, DOI: **10.1029/2007GL031338**.

66 L. Müller, M.-C. Reinnig, K. H. Naumann, H. Saathoff, T. F. Mentel, N. M. Donahue and T. Hoffmann, Formation of 3-methyl-1,2,3-butanetricarboxylic acid via gas phase oxidation of pinonic acid – a mass spectrometric study of SOA aging, *Atmos. Chem. Phys.*, 2012, **12**, 1483–1496.

67 A. Mutzel, M. Rodigast, Y. Iinuma, O. Böge and H. Herrmann, Monoterpene SOA – Contribution of first-generation oxidation products to formation and chemical composition, *Atmos. Environ.*, 2016, **130**, 136–144.

68 A. W. Schroth, J. Crusius, E. R. Sholkovitz and B. C. Bostick, Iron solubility driven by speciation in dust sources to the ocean, *Nat. Geosci.*, 2009, **2**, 337–340.

69 M. Oakes, E. D. Ingall, B. Lai, M. M. Shafer, M. D. Hays, Z. G. Liu, A. G. Russell and R. J. Weber, Iron Solubility Related to Particle Sulfur Content in Source Emission and Ambient Fine Particles, *Environ. Sci. Technol.*, 2012, **46**, 6637–6644.

70 H. O. T. Pye, A. Nenes, B. Alexander, A. P. Ault, M. C. Barth, S. L. Clegg, J. L. Collett Jr, K. M. Fahey, C. J. Hennigan, H. Herrmann, M. Kanakidou, J. T. Kelly, I.-T. Ku, V. F. McNeill, N. Riemer, T. Schaefer, G. Shi, A. Tilgner, J. T. Walker, T. Wang, R. Weber, J. Xing, R. A. Zaveri and A. Zuend, The acidity of atmospheric particles and clouds, *Atmos. Chem. Phys.*, 2020, **20**, 4809–4888.